Flow-induced vibration of an elliptical cylinder and a wake-mounted flat plate

Mohammad Jebelli[a], Koosha Shariloo[b], Mehran Masdari[a]

[a] Faculty of new sciences and technologies, University of Tehran, Tehran, Iran

[b] Department of Aerospace Engineering, Sharif University of Technology, Tehran, Iran

Corresponding author: Mohammad Jebelli

Mailing address:

University of Tehran

Faculty of New Sciences and Technologies

North Kargar Street, Tehran, Iran

E-mail: m.jebelli@ut.ac.ir

Abstract

A numerical simulation is carried out to study flow-induced vibration of an elliptical cylinder equipped with a wake-mounted flat plate in a laminar flow regime at Re=100. The objects are constrained to vibrate independently in the cross-flow direction. The Vortex-induced vibration of an upstream cylinder with four different aspect ratios (AR=0.25, 0.5, 0.75, 1) is investigated in the presence of a plate mounted in different horizontal spacing of G=0.5-3. Simulations are performed for a fixed mass ratio of 10 and negligible damping ratio across a range of reduced velocities (U_r=2-12). The results demonstrate that the presence of the flat plate can amplify the vibration amplitude of the cylinder by altering the shear layers' structure, particularly at short horizontal distances. Moreover, the phase difference of the objects shows a correlation with both the horizontal distance and the AR. Furthermore, the presence of the plate results in broader lock-in regimes across all aspect ratios by delaying its end to larger reduced velocities. While reducing the AR leads to a higher maximum vibration amplitude of the cylinder, it results to a considerably lower amplitude for the plate due to different wake structures and reduced interaction between the shear layers and the flat plate.

Keywords

Flow-Induced Vibration, Vortex shedding, Elliptical cylinder, Flat plate, Laminar flow

1 Introduction

The interaction of fluid flow and bluff structures has been of great interest over the past few decades due to its importance in various engineering applications. It usually comes with a vortex-shedding phenomenon that exerts fluctuating hydrodynamic forces on cylinders immersed in fluid flow. These forces can cause different types of streamwise or transverse vibrations in the objects if they are flexible or just flexibly mounted. The phenomena, known as flow-induced vibration (FIV), on one side, are a concern for the reliability of different industrial structures with cylindrical components, and on the other side, are considered as a new source of clean and renewable energy with the growing shortage of fossil fuels and environmental concerns.

For a circular cylinder as a typical bluff body, the vortex shedding starts as the Reynolds number exceeds 47 and results in a periodic surface loading (Henderson, 1997) and, consequently, a self-sustained oscillation termed vortex-induced vibration (VIV) (Bearman, 1984). When an object is immersed in the wake developed by a bluff body, the upcoming oscillatory forces result in a dynamic response known as wake-induced vibration (WIV), wake-induced galloping, or wake displacement excitation (Zdravkovich, 1988; Bokaian and Geoola, 1984).

Extensive studies and reviews which are performed to develop the knowledge and gain a better insight into different aspects of these phenomena can be divided into three main categories: understanding the phenomena, control and suppression, or enhancing and amplifying the motion. VIV of a circular cylinder has been studied in different aspects, and its mechanisms and fundamental physics are well documented in valuable reviews (Williamson and Govardhan, 2004; Williamson and Govardhan, 2008; Sarpkaya, 2004). Although the results for the VIV of a circular cylinder are sometimes used as the basis for objects with different cross-sections, the associated FIV feature changes significantly in the lack of rotational symmetry.

Based on the cross-section geometry, the cylindrical structures can be divided into three primary categories, including circular and elliptical cylinders with rounded edges and changing separation points, sharp-edged geometries with a fixed one, and the last part, which is a combination of the two first categories like objects with “D” shape or rectangular with rounded-corners cross-sections with varying or fixed separation points (Derakhshandeh and Alam, 2019).

As mentioned earlier, objects with circular cross-sections have received the most attention from researchers. The sharp-edged ones are relatively more explored than the remaining geometries. Due to their structural strength, elliptical structures are becoming more common in the past years (Paul et al., 2014). Geometrical parameters such as aspect ratio (AR) and angle of attack can significantly affect the flow field and make the wake more complex.

Paul et al. studied the variation of the flow field around an elliptical cylinder with different aspect ratios. They classified seven flow regimes for the different combinations of AR, angle of attack, and Re number (Paul et al., 2016). In a numerical study by Johnson et al., vortex shedding occurs differently by changing the AR and Re number. They found that as the AR decreases and Re increases the shedding pattern changes from Karman vortex street to unsteady secondary shedding (Johnson et al., 2001). Faruquee et al. investigated the effect of AR on the flow past an elliptical cylinder with a major axis parallel to the free stream. They showed that the wake structure changes significantly when the AR becomes less than a critical value of 0.34, and selecting higher ARs results in a pair of steady vortices in the wake of the cylinder (Faruquee et al., 2007). The study of Hasheminejad et al. on the VIV of an elliptical cylinder at different inclination angles showed that increasing the AR results in a shift for lock-in phenomena to higher Re numbers (Hasheminejad and Jarrahi, 2015). Zhao et al. found two separated lock-in regimes for an elliptical cylinder with a low AR of b/a=0.67 where a and b are streamwise and cross-flow dimension (Zhao et al., 2019). In the study of Navrose et al., they showed a higher vibration amplitude as the AR increases for the elliptical cylinder whose minor axis is aligned parallel to the free stream (Yogeswaran et al., 2014). Vijay et al. studied the effect of aspect ratio in a Re number and mass ratio of 100 and 10, respectively. The synchronization regime was found to correlate directly to the aspect ratio, and lower ARs not only result in usually a broader lock-in regime but also increase the maximum amplitude for AR=0.1 up to twice of a circular cylinder diameter (Vijay et al., 2020).

Elliptical cylinders are less explored than circular ones, and there are still some unknown aspects of their VIV characteristics. However, by increasing the application of this type of structure, make a change in the flow field, and controlling or enhancing the flow-induced motions attract more attention.

Different methods are used to change the flow field and the response of the objects. Generally, they can be divided into two main categories of active and passive. Flat plates are known as a simple, passive, and effective way among them which are implemented to either suppress or amplify the vortex shedding and flow-induced vibrations. Various studies, including different configurations of a cylinder and flat plates, are conducted to investigate the possible changes in fluid flow.

The first studies in this area date back to 1955 (Roshko, 1955). Stabilizing and narrowing the wake, a delay in vortex shedding, lower shedding frequency, and drag coefficient are the results of installing a flat plate to the rear end of a circular cylinder (Gerrard, 1966; Apelt et al., 1973). The plate's length has a significant effect and may completely suppress vortex shedding for a large enough one (Kwon and Choi, 1996). Utilizing permeable plate and change in the connection angle are also effective in vortex shedding control (Ozkan et al., 2017). A detached plate can also change the base pressure, Strouhal number and even suppress vortex shedding. But its effectiveness strongly depends on the plate's length and the horizontal or vertical location. Utilizing parallel plates is also found effective in drag force reduction by altering the near wake and postponing or even suppressing the vortex shedding (Ozono, 1999; Hwang et al., 2003; Dehkordi and Jafari, 2010).

To find out the effect of a splitter plate on FIVs, Kawai showed that galloping happens for a circular cylinder with an attached plate which is associated with a high amplitude of vibration and a low frequency (Kawai, 1990). Nakamura et al. found that a splitter plate with sufficient length allows galloping start for any bluff body regardless of whether its cross-section is sharp-edged or smooth (Nakamura et al., 1994). Indeed the transition from VIV to galloping happens by increasing the plate length, even for a slotted one (Stappenbelt, 2010; Assi and Bearman, 2015). The lift components generated by the splitter and the cylinder are found as the driving and the suppressing force of galloping, respectively. Therefore, the transition between VIV and galloping results from the competition between these forces (Sun et al., 2020).

Zhang et al. studied the effect of the splitter plate on the torsional free vibration of a cylinder and found that by decreasing the moment of inertia the synchronization range extends and the peak of the VIV amplitude increases. Their study on three degree of freedom cylinder-plate assembly showed three response branches of vertical, torsional and coupled dominated depending on frequency ratio (Zhang et al., 2021a, 2021b). The studies of Jebelli and Masdari showed that simultaneous free and independent vibration of a circular cylinder and a single or parallel downstream flat plates may result in a broader lock-in regime and also a higher maximum vibration amplitude (Jebelli and Masdari, 2022a, 2022b).

On the other hand, using a hinged plate may result in VIV suppression at low reduced velocities (Wu et al., 2014). A wavy plate with a proper length may effectively suppress the initial and lower branches of VIV and also stir the galloping at high reduced velocities (Zhu and Liu, 2020). It can be concluded that utilizing flat plates, whether attached or not, has different and sometimes contradictory effects on the cylinder response, depending on the length, stiffness, location, and type of connection.

In the last decade, FIVs are also considered a new clean and renewable energy source. A piezoelectric plate attached to the rear end of a cylinder is a widespread mechanism of an energy harvesting system that has been investigated in several studies. An et al. proposed a novel method known as VIPEC in which pressure difference induced by shedding vortices drives piezoelectric plate to squeeze and converts the fluid dynamic energy into electrical one (An et al., 2018). A free-to-rotate flat plate elastically mounted in the wake of a modified cylinder is another way examined to extract energy. Although the plate response is found to be independent of the horizontal gap, its efficiency strongly depends on the position of the elastic axis and the spring stiffness (Armandei and Fernandes, 2016).

Based on the above literature, it can be concluded that utilizing flat plates may result in control and suppression or amplifying the flow-induced vibration depending on geometrically and elastically characteristics, and there are still some unknown aspects in their behavior when mounted behind a bluff body. As aforementioned, structures with elliptical cross-sections are also becoming more and more common in different applications. Therefore, study on the effect of a flat plate on the VIV of elliptical cylinders is selected as the aim of the current study.

In the present study, the effect of one downstream flat plate on the VIV of different elliptical cylinders has been investigated numerically. The plate, independently mounted and free to vibrate in the cross-flow direction, is located in different horizontal locations. The paper proceeds by describing the problem, governing equations, and numerical method in section 2, and Section 3 is devoted to numerical model validation. In section 4, numerical results and discussion on simultaneous vibration of an elliptical cylinder and a downstream flat plate are presented. The paper ends with conclusions in Section 5.

Nomenclature

A	Plunging Amplitude
D	Circular Cylinder Diameter
L_P	Flat Plate Length
G	Non-Dimensional Horizontal spacing
m*	Mass Ratio
ζ	Damping Ratio
CL	Lift Coefficient
CL_{RMS}	Root Mean Square of Lift Coefficient
CD_{mean}	Mean Drag Coefficient
Cp	Pressure Coefficient
Cp_b	Base Pressure Coefficient
f	Transverse Oscillation Frequency
f_n	Transverse Natural Frequency
ρ	Fluid Density
m	Body Mass
m_A	Added Mass
K	Transverse Stiffness Factor
U_{in}	Free Stream Velocity
U_r	Reduced Velocity
t	Physical Time
T	Non-Dimensional Time
St	Strouhal Number

2 Problem description and numerical methodology

In this section, the problem of the current study is described in detail, and the governing equations with the numerical methodology utilized for the simulations will be presented.

2.1 Problem description

The focus of the present study is to investigate the effect of a single flat plate mounted in the wake of a cylinder with an elliptical cross-section. The cylinder and flat plate which are independently and elastically mounted, can freely vibrate in cross-flow direction. A mass-spring-damper system models the FIV of the objects with one degree of freedom. A schematic view of the flow passing objects and different ARs of the cylinder are presented in FIG. 1.

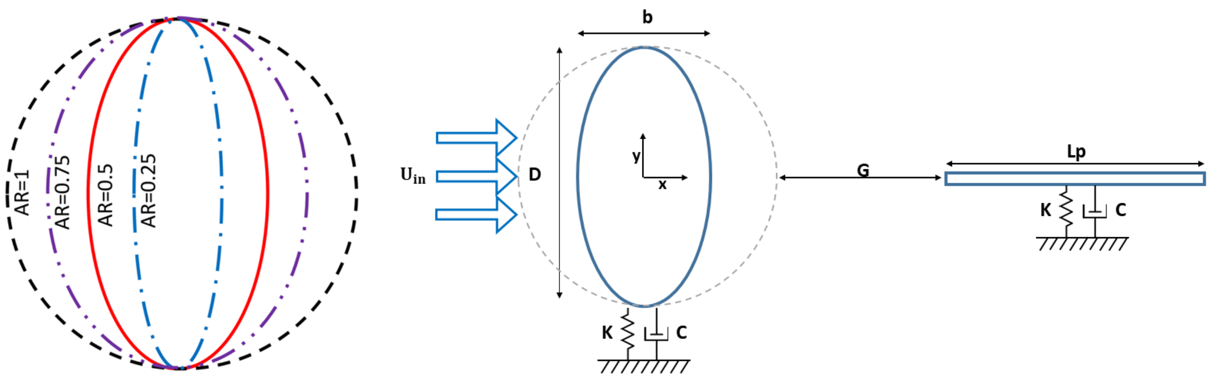

FIG. 1. Schematic view of the flow past a free to oscillate cylinder and a wake-mounted flat plate.

The cylinder's major axis and the plate's length, which are equal, are shown by “D” and “Lp”, respectively. The aspect ratio of the cylinder is based on the minor axis width over the major one (AR=b/D). “G” represents the non-dimensional horizontal distance between the objects, and the thickness of the plate is set as δ=0.03D.

The dynamic response of a system with FIV depends on different parameters including the Reynolds number, the mass and damping ratio. The mass ratio defines as $m^* = m/m_A$ based on the mass and added mass of the body. The damping ratio defines as $\zeta = c\ /\ (2\sqrt{mk})$ where "c" and "k" are the damping and spring stiffness of the elastically mounted object.

In the wake of a circular cylinder, the flow transition occurs when the Re number of the free stream is larger than 180 (Williamson, 1996; Jiang et al., 2016). Study on the effect of the cylinder's aspect ratio on the Strouhal number showed different wake structures including re-laminarization for AR<0.4 (Radi et al., 2013). Therefore, to avoid three-dimensionality effects, a Reynold number of 100 ($Re = \rho U_{in} D/\mu$) is selected for all cases that allows the utilization of a two-dimensional (2D) simulation method.

As the primary goal of the current study is to determine the effects of the horizontal location of the downstream plate and the AR of the cylinder on the wake structure and simultaneous FIV of the objects, the mass ratio and Re number are kept constant at 10 and 100, respectively. As the flow velocity (U_{in}) is fixed, the reduced velocity ($U_r = U_{in}/f_n D$) varies by changing the natural frequency. The spring stiffness also varies in different cases as the natural frequency changes. Finally, the structural damping ratio is set as zero to encourage a high amplitude vibration. The non-dimensional parameters of the simulations are summarized in the TABLE I.

TABLE I. Main simulation parameters.

Parameter	symbol	value
Mass ratio	m*	10
Damping ratio	ζ	0
Horizontal distance	G=L/D	0.5-3
Reynolds number	Re	100
Aspect ratio	AR	0.25, 0.5,0.75, 1

2.2 Governing Equations

As a low Re number of 100 is applied in this work, resulting in a laminar flow field, the 2D incompressible, unsteady Navier-Stokes equations are used to model the flow field around the objects. The related conservation of mass and momentum equations are presented as follows (White, 1994):

$$\frac{\partial u^*}{\partial x^*}+\frac{\partial v^*}{\partial y^*}=0 \tag{1}$$

$$\frac{\partial u^*}{\partial t^*}+u^*\frac{\partial u^*}{\partial x^*}+v^*\frac{\partial u^*}{\partial y^*}=-\frac{\partial p^*}{\partial x^*}+\frac{1}{Re}\left(\frac{\partial^2 u^*}{\partial x^{*2}}+\frac{\partial^2 u^*}{\partial y^{*2}}\right) \tag{2}$$

$$\frac{\partial v^*}{\partial t^*}+u^*\frac{\partial v^*}{\partial x^*}+v^*\frac{\partial v^*}{\partial y^*}=-\frac{\partial p^*}{\partial y^*}+\frac{1}{Re}\left(\frac{\partial^2 v^*}{\partial x^{*2}}+\frac{\partial^2 v^*}{\partial y^{*2}}\right) \tag{3}$$

In equations (1), (2), and (3), the dimensionless variables are evaluated as follows:

$$x^*={}^{x}/_{D}\quad y^*={}^{y}/_{D}\quad u^*={}^{u}/_{U_{in}}\quad v^*={}^{v}/_{U_{in}}\quad p^*={}^{p}/_{\rho U_{in}{}^2}\quad t^*={}^{t}/_{U_{in}D}$$

In the above equations, "u" and "v" denote the flow velocity components in streamwise and transverse directions, respectively. "t" is the real flow time, "ρ" is the fluid density, , "D" is cylinder major axis, "U_{in}" is the flow velocity at inlet and "p" represents the static pressure.

The equation (4) of motion presents the mechanical response of the mass-spring-damper model:

$$m\ddot{Y}+2m\zeta\omega_0\dot{Y}+m\omega_0^2Y=f_l(t) \tag{4}$$

Y, $\dot{Y}$ and $\ddot{Y}$ denotes the transverse displacement, velocity, and acceleration of the structure respectively. $\omega_0=2\pi f_n$ is the natural circular frequency of the object and finally the $f_l(t)$ is the time dependent lift force in cross-flow direction. The SIMPLE algorithm is used for coupling the pressure and the velocity vector. The second-order upwind and the least-squares cell-based schemes are utilized to discretize the convective and gradient terms, respectively.

2.3 Numerical Method

In the present study, the numerical simulation is conducted using ANSYS Fluent as a reliable CFD software. In an FIV case, the objects are free to oscillate; thus, a dynamic mesh is required, which adapts itself with the moving objects at each time step. An arbitrary Lagrangian-Eulerian method is utilized in ANSYS Fluent which includes three dynamic mesh schemes, namely smoothing, layering, and remeshing. A diffusion-based smoothing method is used for the present study, which is accompanied by a user-defined function (UDF) to connect the structural and fluidic parts.

Different studies showed that the computational domain size, particularly the blockage effect, can significantly change the simulation results. An error in predicting the forces may appear if a small domain is selected. For the case of VIV of a cylinder, vibration in cross-flow direction can intensify the errors. In this regard, the blockage is likely to play an even more important role in the simulation of FIV cases. Prasanth and Mittal showed that a computational domain with a blockage of more than 2.5% for a circular cylinder might leads to hysteresis in vibration response at the beginning of the lock-in regime. Setting the lateral boundaries with a blockage of 2% seems proper for the VIV of two circular cylinders in tandem and staggered arrangements (Prasanth et al., 2006; Prasanth and Mittal, 2008, 2009); Therefore, it is selected for the current study. Considering the above, the simulation domain size, the model's geometry and the boundary conditions are presented in FIG. 2. The computational domain consists of a rectangular with 75D and 50D in streamwise and cross-flow directions. The cylinder center is set as the origin of the coordinate system, located 25D away from the inlet boundary. Finally, the lateral bounds of the domain are defined at 25D from the cylinder center (equivalent to a blockage of 2%) to avoid any computational errors.

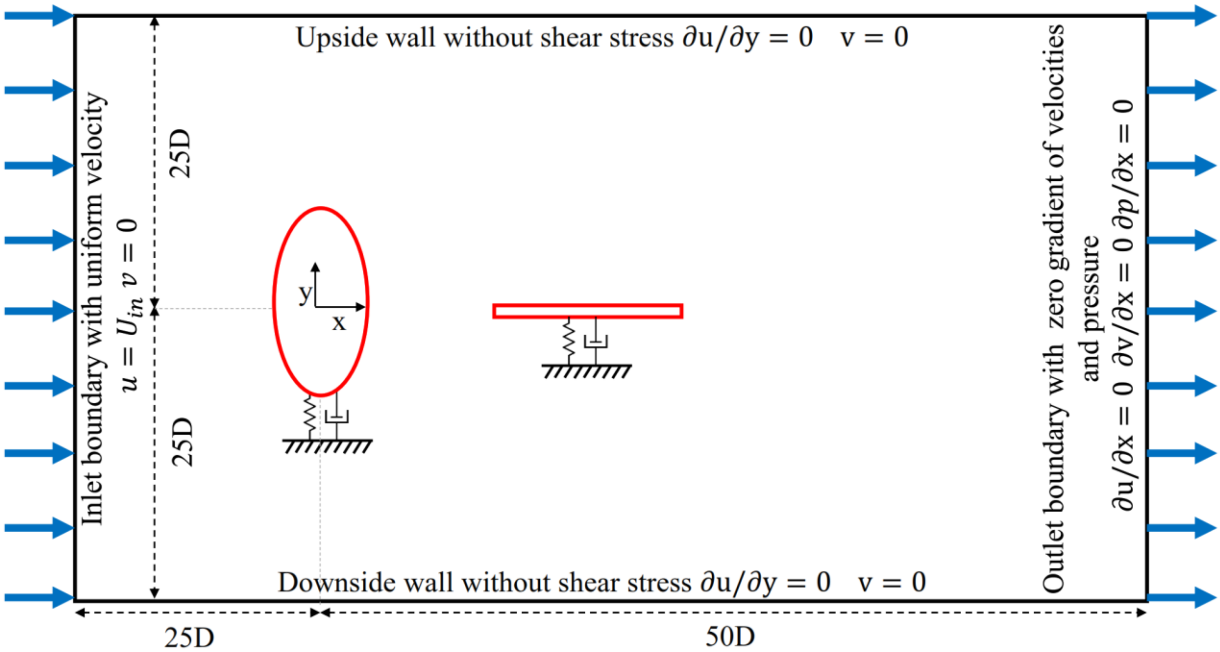

FIG. 2. Schematic of CFD model around an elliptical cylinder and the parallel plate including domain and boundary conditions.

A uniform velocity is defined for the flow at the inlet boundary. Zero normal gradient is specified for the velocity at the outlet, and the pressure is defined with a reference value of zero. In the lateral bounds, the stress vector along the boundary and the normal term of the flow velocity are zero. A no-slip condition is set for the surfaces of the cylinder and the flat plate.

2.4 Computational domain and mesh dependency

Grid independency and temporal resolution validation are required prior to the detailed study of the main cases. FIG. 3, as an example, shows the generated grid around the elliptical cylinder with an AR of 0.5 and the downstream flat plate mounted at G=1.

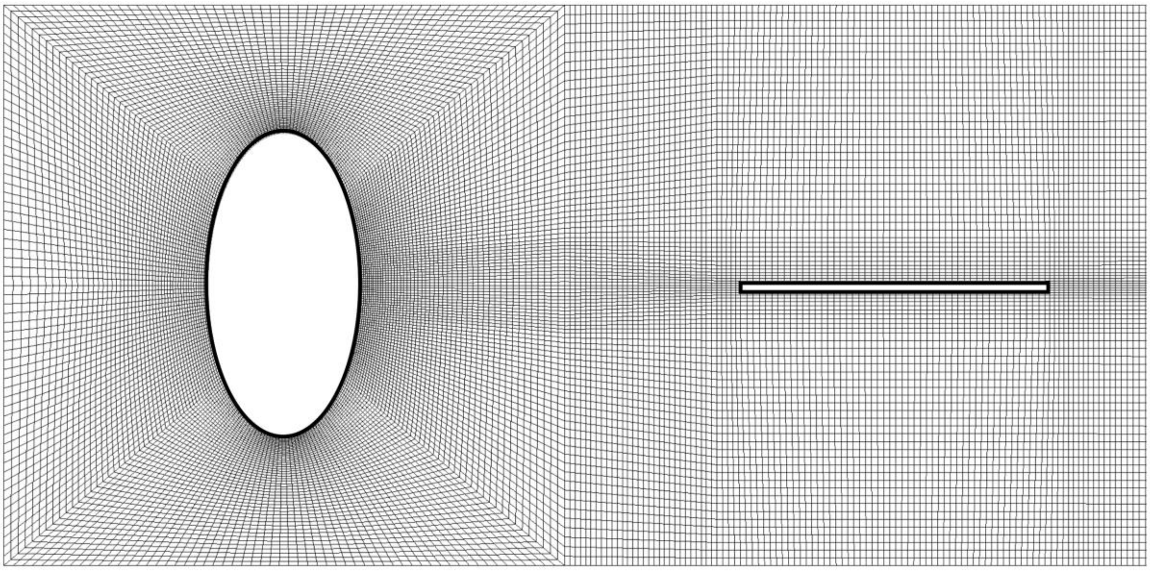

FIG. 3. Typical mesh elements in CFD model for the case of elliptical cylinder with AR=0.5 and the flat plate at G=1.

The cylinder surface is divided into four sections: front, top, bottom, and finally the rear side, which among them the last one is more important due to the high flow gradients of the near wake. The presence of the flat plate also results in a more complex local flow. The grid is condensed around the objects and also gradually coarsened in the regions far from them to reduce the computational cost. The mesh independency study is conducted for two configurations. The first one deals with one degree of freedom VIV of an elliptical cylinder in cross-flow direction and the second one includes the simultaneous FIV of an upstream circular cylinder with one downstream flat plate mounted in the wake. The grids are generally similar in both configurations. However, the second one includes more cells in the cylinder wake due to the presence of the flat plate and more complexity of the flow in that region.

In TABLE II, the transverse displacement, root mean square of the lift coefficient and mean drag coefficient for an elliptical cylinder with an aspect ratio of 0.5 are presented. The percentage deviation of the parameters is indicated inside the brackets. According to the results, grid G-1-2 provides independent results for the case of a bare elliptical cylinder (AR=0.5), and higher grid resolutions result in a deviation of less than 2 percent.

TABLE II. Grid independency study for VIV of an elliptical cylinder (AR=0.5, Re=100, Ur=6).

Grid	Cylinder Nodes	Y_{max}	CL_{RMS}	CD_{RMS}
G-1-1	200	0.45	0.38	0.277
G-1-2	240	0.43 (4.44%)	0.36 (5.26%)	0.269 (2.97%)
G-1-3	260	0.425 (1.16%)	0.353 (1.94%)	0.267 (0.74%)

As the primary goal of the current study is to investigate the effect of a wake-mounted flat plate on an elliptical cylinder, a grid dependency study is necessary for this configuration. Due to high flow gradients and the complexity of the flow, more cells are required between the rear side of the cylinder and the flat plate. Therefore, new grids with similar structures but more cells on the cylinder's rear side, are generated for the last case of the grid dependence study. Corresponding results are presented in TABLE III.

TABLE III. Mesh resolution sensitivity examinations for the VIV of an elliptical cylinder and a downstream flat plate (AR=0.5, G=3, Re=100, Ur=6).

Grid	Cylinder Nodes	Ellipse (AR=0.5)			Flat Plate		
		Y_{max}	CL_{RMS}	CD_{mean}	Y_{max}	CL_{RMS}	CD_{mean}
G-2-1	180+60	0.57	0.41	2.3	0.28	0.48	0.157
G-2-2	180+70	0.53 (7%)	0.38 (7.3%)	2.27 (1.3%)	0.26 (7.1%)	0.44 (8.3%)	0.153 (2.5%)
G-2-3	180+80	0.52 (1.8%)	0.371 (2.3%)	2.25 (0.8%)	0.255 (1.9%)	0.424 (3.6%)	0.15 (1.9%)
G-2-4	180+90	0.52 (0%)	0.368 (0.8%)	2.246 (0.2%)	0.252 (1.2%)	0.417 (1.65%)	0.15 (0%)

Comparing the results, including the maximum transverse amplitude, root mean square of the lift and mean drag coefficients show that the grid G-2-3 has a small enough deviation, ensuring the grid independency. Therefore, this grid is selected for further simulations. The non-dimensional time step ($t_{non-dimensional} = tU/D$) is chosen to be equal to $\Delta t = 0.002$ based on a temporal resolution analysis that also satisfies the Courant-Friedrichs-Lewy ($CFL < 1$) number by employing the selected grid.

3 Numerical model validation

In order to validate the accuracy of the computational approach, the VIV of an elliptical cylinder with two different aspect ratios (AR=0.25, 0.5) for a mass ratio and Re number of 10, 100 respectively, are simulated and compared with the related references. FIG. 4 presents the variation of the maximum amplitude of the elliptical cylinder for a range of reduced velocities.

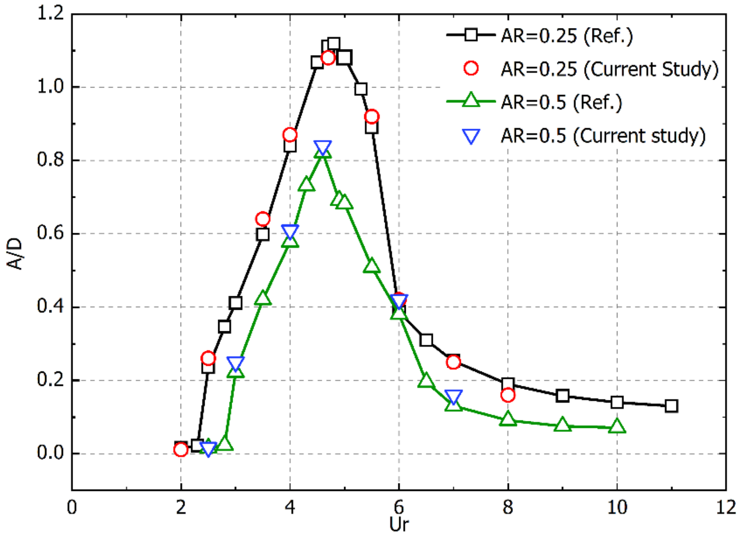

FIG. 4. Variation of dimensionless vibration amplitudes for the cylinder for AR=0.25, 0.5 (mean values of the top 10% of response amplitudes) (Vijay et al., 2020)**.**

By reducing the AR from 0.5 to 0.25, the maximum amplitude rises considerably, and the synchronization regime starts slightly sooner. Both are predicted accurately in the current simulations and are in good agreement with the reference (Vijay et al., 2020). Additionally, root mean square (RMS) values of lift coefficient are also compared in FIG. 5.

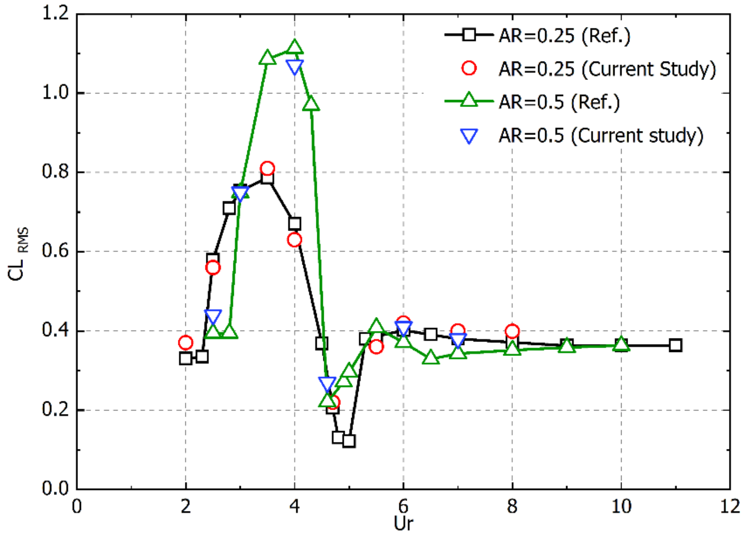

FIG. 5. Variation of RMS values of lift coefficient for the cylinder for AR=0.25, 0.5 (Vijay et al., 2020)**.**

Comparing the results with the reference shows that the utilized numerical approach is adequate enough to settle the VIV of elliptical cylinders. The next part of the validation procedure deals with the simultaneous free vibration of an upstream circular cylinder with a wake-mounted flat plate. The authors in their previous study (Jebelli and Masdari, 2022a) numerically simulated the VIV and WIV of a circular cylinder and a flat plate. Therefore, a similar approach will be used here.

4 Results and discussions

This section presents the results of the simultaneous FIV of a single wake-mounted flat plate and an upstream elliptical cylinder. The first part of the section presents the results for different geometrical configurations achieved by varying the aspect ratio of the cylinder and the horizontal spacing between the two objects. In the second part, the FIV response of selected configurations is analyzed across a range of reduced velocities to determine the effect of small spacing on the vibration of the objects.

4.1 Simultaneous FIV in Different Configurations

The simultaneous free vibration of an upstream cylinder and the flat plate are conducted for different configurations and a fixed reduced velocity of U_r=6 as it is in the synchronization regime for most similar geometries. The natural frequency of all objects is set based on the vortex shedding frequency of a fixed circular cylinder at a Re number of 100, and the horizontal gap between the objects varies in a range of G=0.5-3. FIG. 6 presents the vibration amplitude of the upstream cylinder (a) and the downstream flat plate (b) in different configurations.

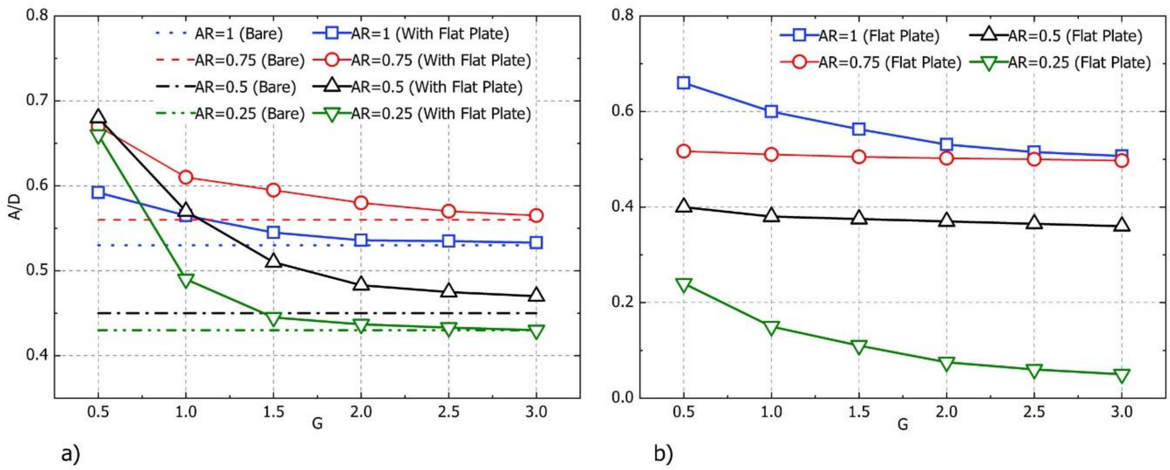

FIG. 6. Vibration amplitude of a) the upstream cylinder and b) the flat plate for different horizontal spacing at U_r=6.

The vibration amplitude of the cylinder can be discussed in two aspects: the variation of maximum amplitude and its rate of change. When the flat plate is mounted at G=3, it has minor or even negligible effects on the cylinder. However, a reduction in the horizontal gap (G) leads to gradual growth in vibration amplitude for all ARs (FIG. 6–a). Maximum amplitude in each AR appears for the shortest gap, and the case of AR=0.5 has the largest one reaching up to A/D=0.72. In opposition, a circular cylinder (AR=1) has the lowest maximum amplitude with A/D=0.59. For the flat plate (FIG. 6–b), an AR reduction clearly leads to lower amplitudes. A flat plate mounted in the wake of a circular cylinder (AR=1) has the largest amplitude, reaching up to A/D=0.66. Changing the AR to 0.25 results in a considerably lower amplitude that does not exceed A/D=0.23 at any horizontal spacing.

By considering the rate of change, it is clear that reducing the AR results in more VIV amplification for the cylinder in shorter gaps (FIG. 7-a). While the cylinder in every AR vibrates with an almost identical amplitude for G=3, the reduction of G leads to only an 11% higher amplitude for AR=1. It is about 18% for AR= 0.75, and selecting AR=0.5 and AR=0.25 results in about 51% and 54% higher vibration amplitudes, respectively.

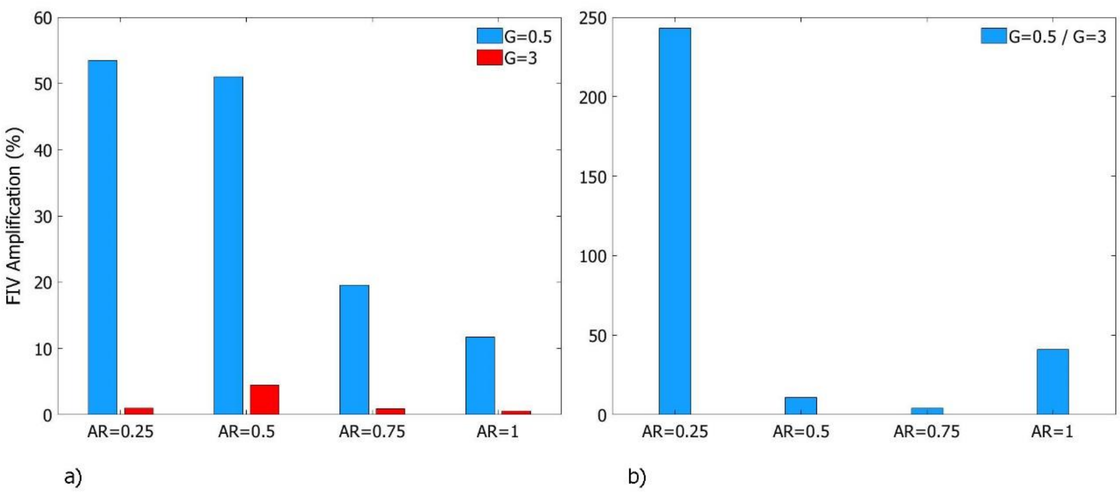

FIG. 7. Change in vibration amplitude: a) the cylinder compared with a bare one b) the flat plate at G=0.5 comparing with G=3

The rate of change for the flat plate is found differently. Reduction of G for AR=0.25, 1 leads to higher vibration amplitudes up to 40% and 242%, respectively (FIG. 7-b). In opposition, this effect would be negligible for AR=0.5, 0.75, in which the plate vibrates with relatively constant amplitudes in different spacings. It is worth noting the FIV response of the objects may vary in different reduced velocities depending on their synchronization regime. But Ur=6 in most cases is a common velocity in top or middle of lock-in range. FIG. 8 shows the vibration phase difference between the objects.

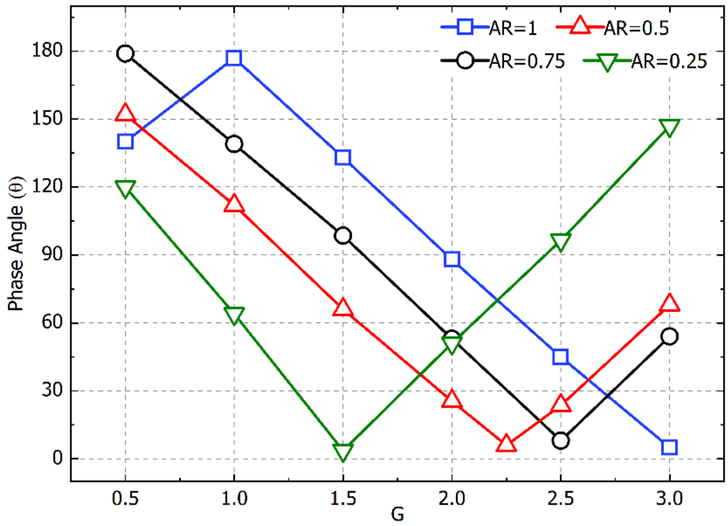

FIG. 8. Vibration phase difference between the cylinder and downstream flat plate.

The results show a direct correlation between the phase angle and the horizontal gap. For the case of AR=1, increasing the gap at first leads to the highest phase difference (about 180˚), then it decreases linearly up to G=3 in which the objects' vibration is almost in-phase. Reduction of AR shifts the location with the lowest phase difference to the smaller horizontal spacing of G=2.5, 2.25, and 1.5 for configurations with an AR of 0.75, 0.5, and 0.25, respectively. As a result of reducing the AR by half, the location of the in-phase vibration moves toward the cylinder by 0.75D. The instantaneous vorticity contours at these critical points are presented in FIG. 9.

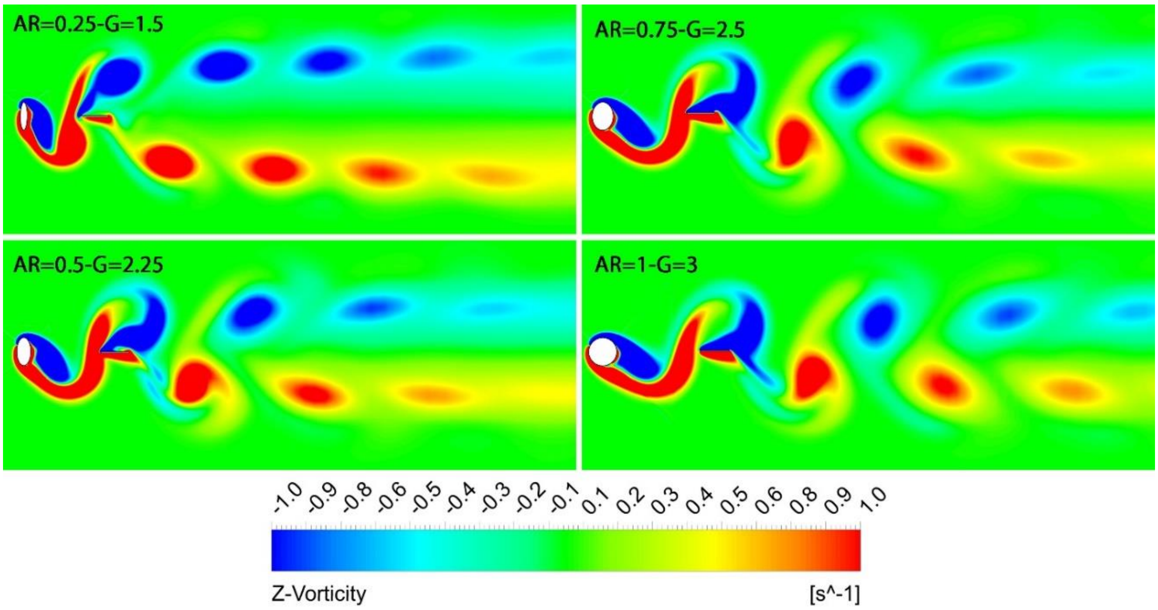

FIG. 9. Instantaneous vorticity contours in different configurations at an identical moment (A/D Cylinder=0).

It is clear that a reduction in the AR of the upstream cylinder changes the vortex formation and shedding mechanism in a way that shortens the location of in-phase vibration. Comparing the cases of AR=0.25, 1 shows that the shear layers in the lower ARs form a bit more vertically. They interact with each other slightly sooner which subsequently results in shorter vortex shedding length.

As mentioned earlier, lower horizontal gaps amplify the vibration amplitude, especially for the upstream cylinder. Changes in the near wake structure are expected to be the reason behind the amplification. In FIG. 10, variation of the pressure coefficient of the cylinder and the near wake structure are presented for AR=0.25-G=0.5,3 and AR=1-G=0.5,3.

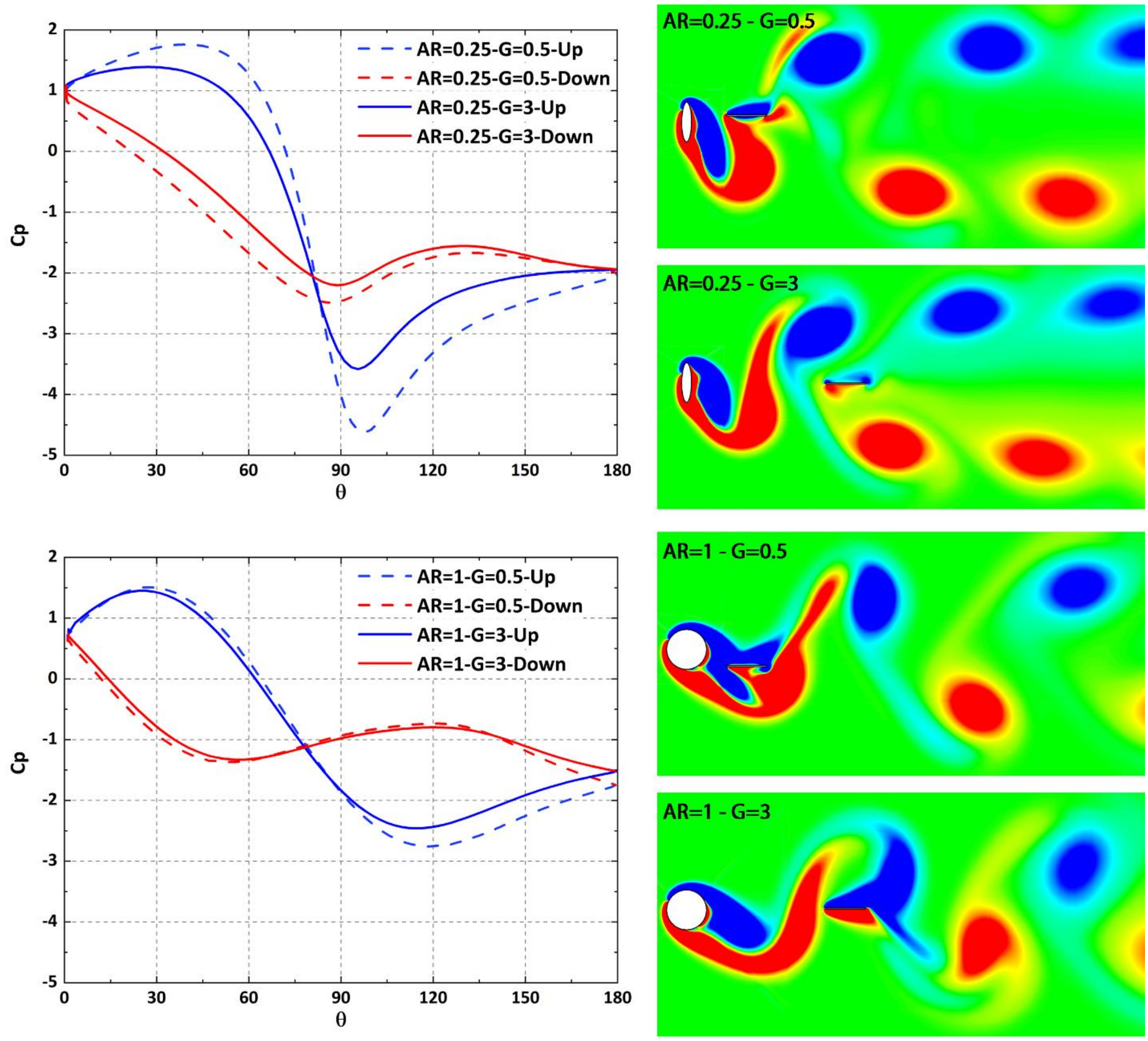

FIG. 10. Instantaneous vorticity contours and pressure coefficient distribution over the cylinder for AR=0.25, 1 and G=0.5, 3.

As the flat plate moves to G=0.5, the vortex formation structure changes. A closer look into the flow between the objects reveals that the plate changes the shear layers' structure and forces them to form a bit closer to the rear end of the cylinder. This new position makes some changes on the upper and lower sides of the cylinder. A slightly higher pressure difference on the cylinder's front side (ϴ=0-90) can be seen in both diagrams which is more significant for AR=0.25. However, the main effect is found on the rear-upper side where the Cp falls, especially for the lower AR. This flow structure results in higher lift and consequently amplifies the VIV of the cylinder.

FIG. 11, compares the bare cylinder and case G=0.5, including the phase relation between oscillation and lift force for one cycle of cylinder vibration. Streamlines, pressure coefficient, and spanwise vorticity contours are also presented at T=0.4 of a vibration cycle. Although the plate changes the near wake structure at every moment of a cycle, comparing the lift shows a secondary peak at T=0.4. Therefore this unique time step is selected to reveal the origin of the phenomena.

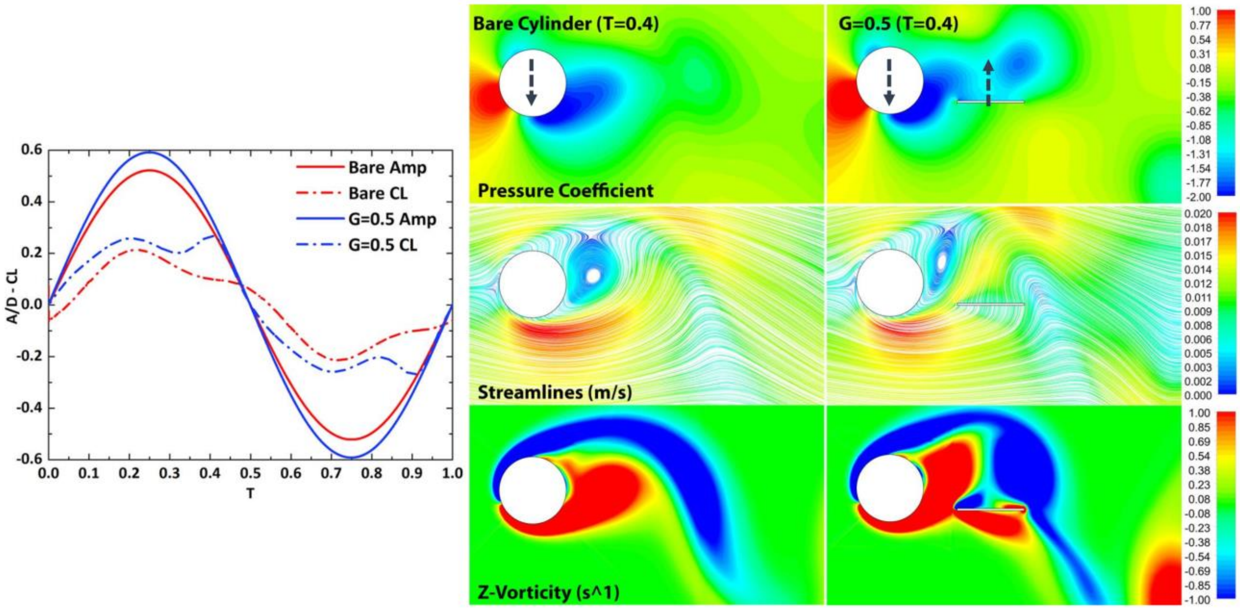

FIG. 11. Phase relation between oscillation and lift force for one cycle of cylinder vibration (AR=1-U_r=6), and pressure coefficient, streamlines and vorticity contours at T=0.4.

The new wake structure includes a stretched vortex at the back side and flow acceleration at the bottom of the cylinder. Higher pressure from the stagnation to the bottom and slightly lower pressure at the upper-rear side of the cylinder, which the latter is the direct result of the stretched vortex, results in a higher lift coefficient at this unique moment. Based on the significant motion phase difference between the objects (about 140˚), this phenomenon happens about 40 and 90 percent of one cycle of cylinder oscillation for the lower and upper shear layers, respectively, resulting in a secondary peak for the cylinder lift coefficient.

4.2 Amplitude Response and hydrodynamic forces

This section explores the simultaneous free vibration of two objects across a range of reduced velocities to determine the FIV response, particularly on the lock-in regime. To minimize computational costs, simulations are conducted for a small horizontal spacing of G=0.5, which, according to the results of the previous section, generally amplifies FIV. In FIG. 12, the normalized vibration amplitudes in transverse direction for the cylinder and the flat plate are presented in different ARs.

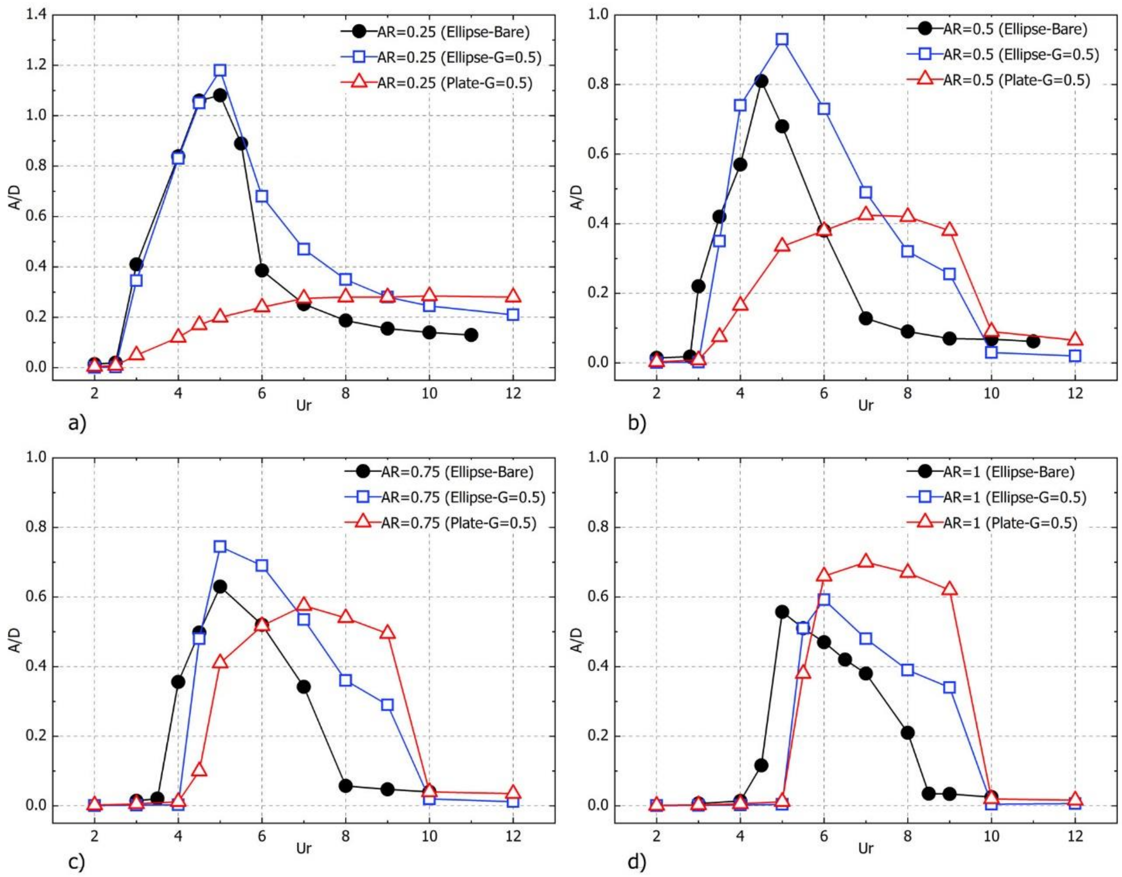

FIG. 12. The amplitude response of the cylinder and the flat plate in different ARs.

When AR=0.25 (FIG. 12-a), the presence of the flat plate has no considerable effect on the response of the upstream cylinder for low reduced velocities (U_r<6); the cylinder's amplitude jumps for U_r=3 and rises up to U_r=5. While higher reduced velocities come with a reduction in maximum amplitude, it falls with a lower rate, and relatively higher amplitudes appear in presence of the plate (A/D=0.25 vs. A/D=0.14 at U_r=10). The plate behaves differently, and its vibration amplitude rises gradually by increasing the reduced velocity, reaches up to about A/D= 0.3, and remains almost constant for a wide range.

For AR=0.5 (FIG. 12-b), the rise in vibration amplitude of the cylinder happens at an almost similar reduced velocity, but the maximum, which is about 15% higher than a bare one, occurs at U_r=5 instead of U_r=4.5. A wider lock-in regime that leads to higher amplitudes for the range of reduced velocities (U_r=6-9) also appears in this configuration. For U_r≥10, the cylinder vibration weaken and the amplitude falls to an even lower value compared to a bare cylinder. The plate's vibration response is basically different, including a gradual increment for U_r≥3.5, a maximum amplitude of A/D=0.46 at U_r=7, and after a slight reduction, it finally falls at U_r=10.

When AR=0.75 (FIG. 12-c), by mounting the flat plate, the synchronization for the cylinder starts at a bit larger reduced velocity of U_r=4.5 (instead of U_r=4) and continues with a maximum vibration amplitude of about 18% larger than the bare cylinder (at U_r=5). This configuration also results in a relatively broader lock-in regime which includes a gradual amplitude decline for higher velocities which ends at U_r=10 (instead of U_r=8). The plate's vibration starts at a similar velocity (U_r=4.5) and gradually rises up to A/D=0.57 for U_r=7. Increasing the velocity comes with lower vibration amplitudes, and finally, it falls at U_r=10 which is matched with the upstream cylinder.

For AR=1 (FIG. 12-d), the presence of the flat plate at G=0.5 delays the beginning of the lock-in regime and the start of VIV, and the maximum amplitude of the cylinder occurs at U_r =5.5 and t U_r=6, respectively. The amplitude gradually decreases up to U_r=9, and the vibration disappears for U_r=10. The response of the flat plate is generally similar to the upstream cylinder in terms of the beginning and end of the lock-in regime. Except its amplitude is relatively constant during the lock-in regime.

In general, the main effect of the flat plate is to widen the synchronization regime regardless of the AR. A slightly shift in the beginning of lock-in regime and a higher maximum vibration amplitude are also appeared by presenting the flat plate in some cases. Although lowering the AR amplifies the vibration amplitude of the cylinder considerably, it reduces the flat plate amplitude. Considering these effects, a combination of a low AR and a near-wake mounted flat plate results in a system that may have great potential for harvesting energy. The variation of frequency ratio in different ARs are presented in FIG. 13.

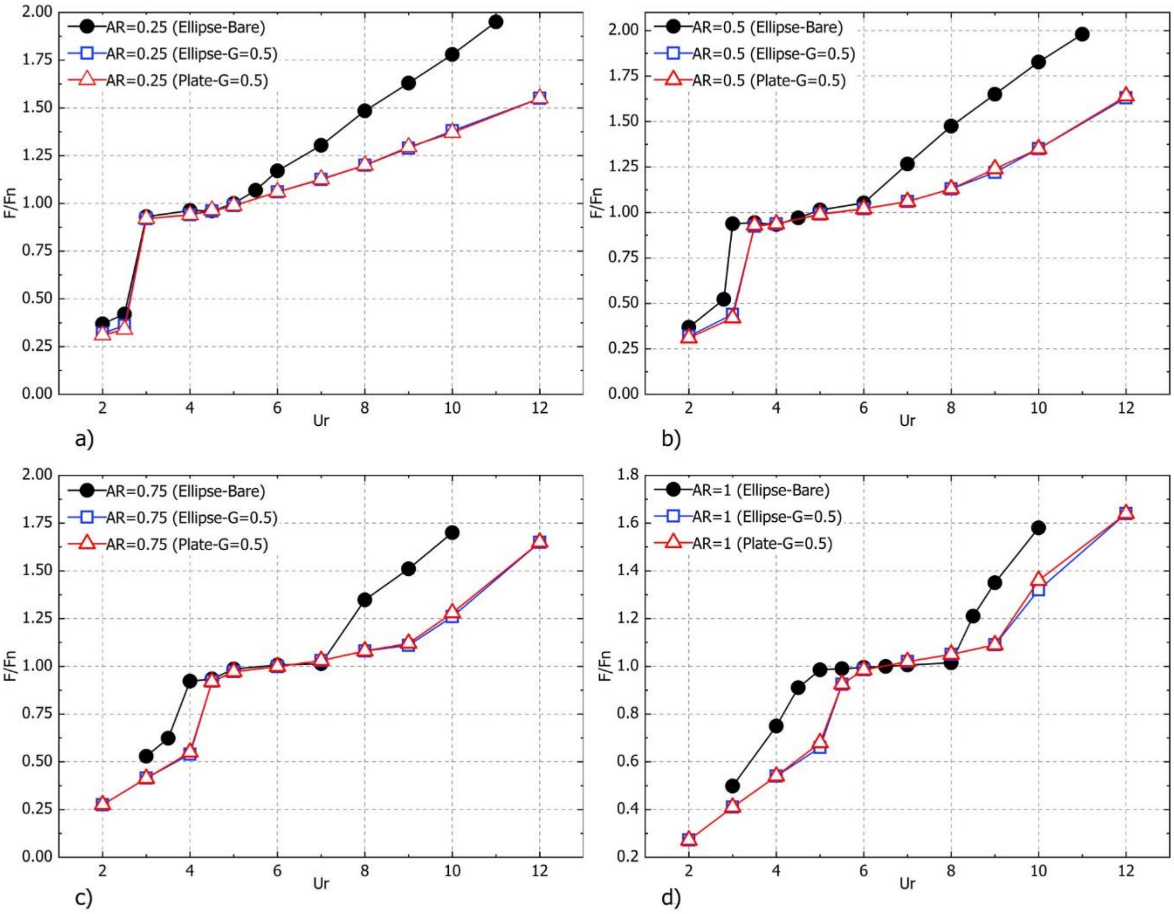

FIG. 13. The frequency ratio of the cylinder and the flat plate in different ARs.

As expected, the frequency ratio of the cylinder changes in the flat plate's presence. The synchronization of the cylinder with AR=0.25 (FIG. 13-a) starts at U_r=3, approaching F/F_n=1, in the presence or absence of the flat plate. While the end of the lock-in regime can usually be identified by a sudden increase in frequency ratio, it is noteworthy that the jump at the end of the lock-in regime disappears for AR=0.25, and the frequency rises at a low rate as the velocity increases. When AR=0.5, A small shift at the beginning of the lock-in regime (U_r=3.5 instead of U_r=3) and a gradual increase of the frequency ratio in higher reduced velocities are also found (FIG. 13-b).

For AR=0.75 (FIG. 13-c), while the frequency ratio of the bare ellipse jumps at U_r=4, it remains about 0.5 for the cylinder and flat plate in simultaneous vibration, and the jump occurs at U_r=4.5. The frequency ratio remains around one for all objects up to U_r=7. While higher reduced velocities result in larger vibration frequencies for the bare cylinder, which confirms the end of synchronization, it remains close to one and begins to rise at U_r=10 in the presence of the flat plate. For the case of AR=1 (FIG. 13-d), a shift in the start of the lock-in (U_r=5.5 instead of 4.5) and end of synchronization (U_r=10 instead of 8.5) is also visible which is matched with the vibration amplitude. The vibration frequency of the flat plate follows the upstream cylinder in all cases. The variation of CL_{RMS} shows that the lift force may vary considerably in different ARs (FIG. 14).

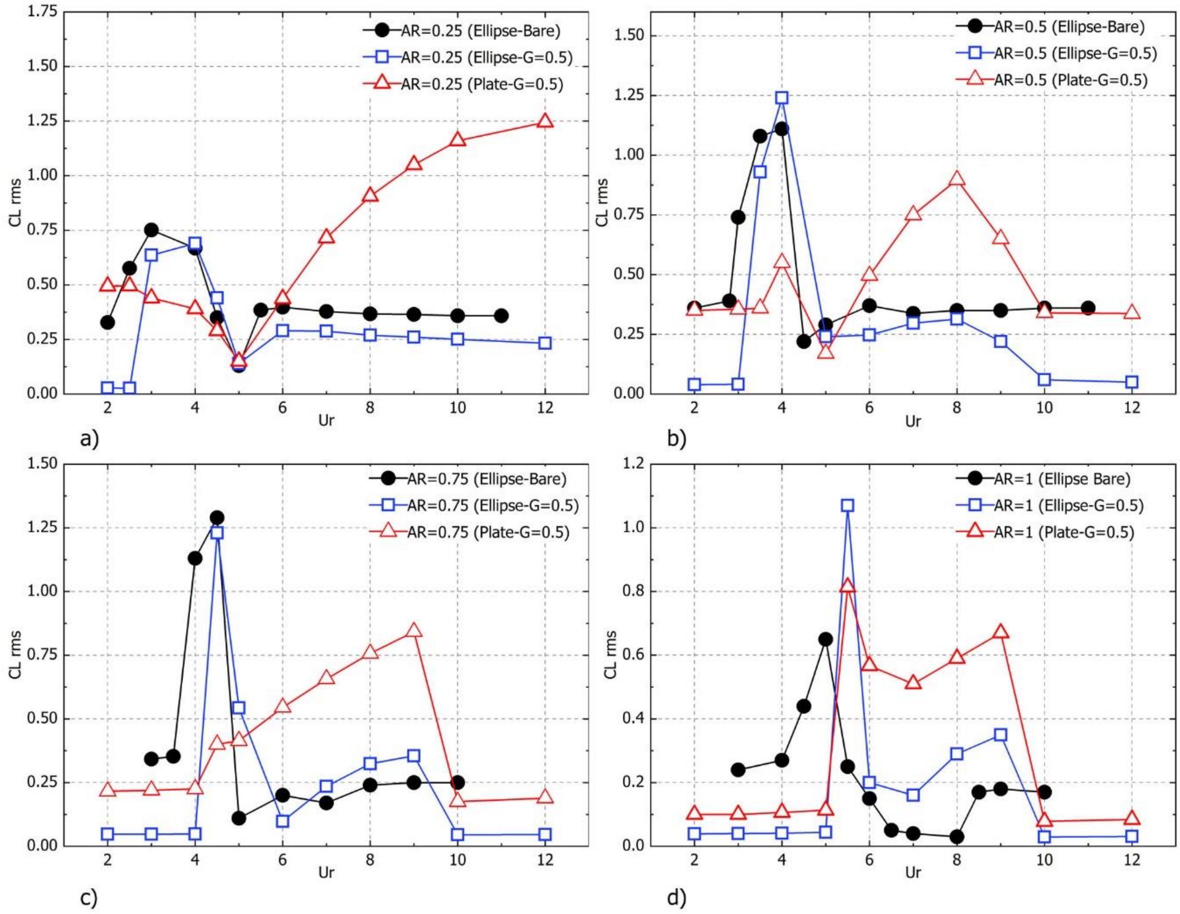

FIG. 14. The CL_{RMS} of the cylinder and the flat plate in different ARs.

For the lowest Aspect ratio (AR=0.25), although the CL_{RMS} of the cylinders has not changed significantly, except for U_r=2,2.5, the lift force of the plate behaves differently. It gradually decreases in the range of U_r=2-5 and then grows sharply for higher reduced velocities (FIG. 14-a). When AR=0.5 (FIG. 14-b), the Lift coefficient shows a similar trend for the cylinder in the presence or absence of the flat plate. The CL_{RMS} for the plate shows an initial rise and then a sudden fall for U_r=5. Higher velocities result in significant growth, and finally CL_{RMS} falls and remains about 0.35 for U_r>10.

When the AR changes to 0.75 (FIG. 14-c), although the CL_{RMS} of the cylinder shows a similar behaviour, except outside of the lock-in regime, it is different for the flat plate in which rises gradually up to U_r=9 and then falls drastically. For a circular cylinder (FIG. 14-d), while the

CL_{RMS} of the bare cylinder gradually rises by increasing the velocity and reaches its maximum, it is considerably lower and almost constant in the presence of a flat plate for U_r=2-5 and then jumps suddenly. The maximum value for the cylinder is higher in simultaneous vibration and appears in a larger reduced velocity which is consistent with the vibration response. Larger reduced velocities first come with a sudden fall, and then a gradual increase of CL_{RMS} is visible for all objects. By the end of the lock-in regime, the lift of the bare cylinder is considerably higher than those of the cylinder and the flat plate in simultaneous vibration, which shows a sudden fall (U_r>10). In fact presence of the flat plate results in lower CL_{RMS} for the cylinder in all ARs outside the lock-in regime. This phenomena would be discussed in the next section. In figure FIG. 15, the vibration phase difference between the objects is presented for different reduced velocities.

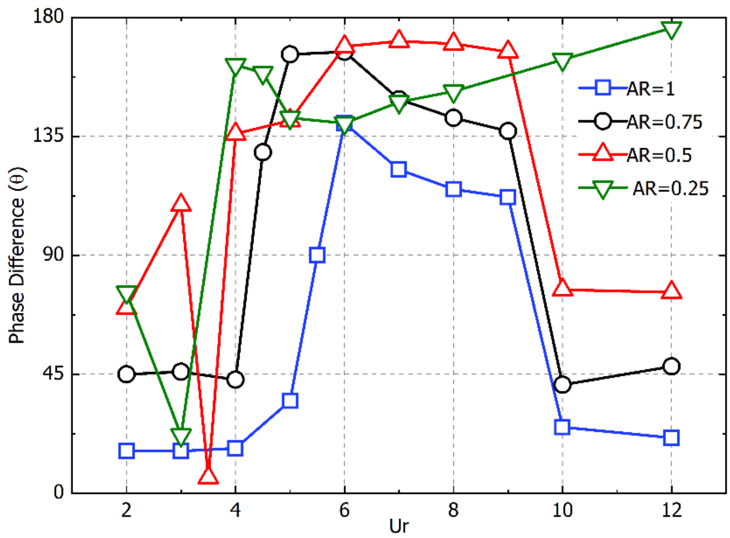

FIG. 15) Vibration phase difference between the cylinder and flat plate in different reduced velocities at G=0.5

According to the results, the phase difference between the objects is generally small for the reduced velocities out of the lock-in regime. A sudden jump and fall appear at the start and end of synchronization (Except for AR=0.25). As shown earlier, the variation of the lift coefficient is also lower in these regions. The symmetric wake around the objects and delay in vortex shedding are found as the reason behind the phenomenon (discussed in the next section). As the aspect ratio reduces (AR=1, 0.75, 0.5), a relatively higher phase lag is found in almost all reduced velocities. It can be addressed to larger gap between the objects due to the change in the shape of upstream objects and consequently the shear layers.

When AR is set to 0.25, 5 a sudden fall is observed for U_r=3, 3.5 respectively which in both cases, these velocities are associated with the start of vibration. The phase difference for AR=0.25 is found to be significantly different in higher velocities. While in other ARs, the phase lag falls at the end of lock-in, it rises continuously, reaching about 180 at U_r=12.

4.3 Wake Structure

Upon closer examination of the wake, it becomes apparent that while a change in aspect ratio leads to different wake patterns, the structure of the wake can be divided into two parts. The primary difference lies in the velocities associated with the start of vibration and the initial response branch. In the case of AR=1, as depicted in FIG. 16, the flat plate present in the wake delays the shedding of vortices beyond the flat plate at low reduced velocities (AR=1 - U_r=2-5). This flow structure results in small variations of the lift coefficient during one oscillation cycle, and consequently the vibration amplitude would be negligible (shown in FIG. 12).

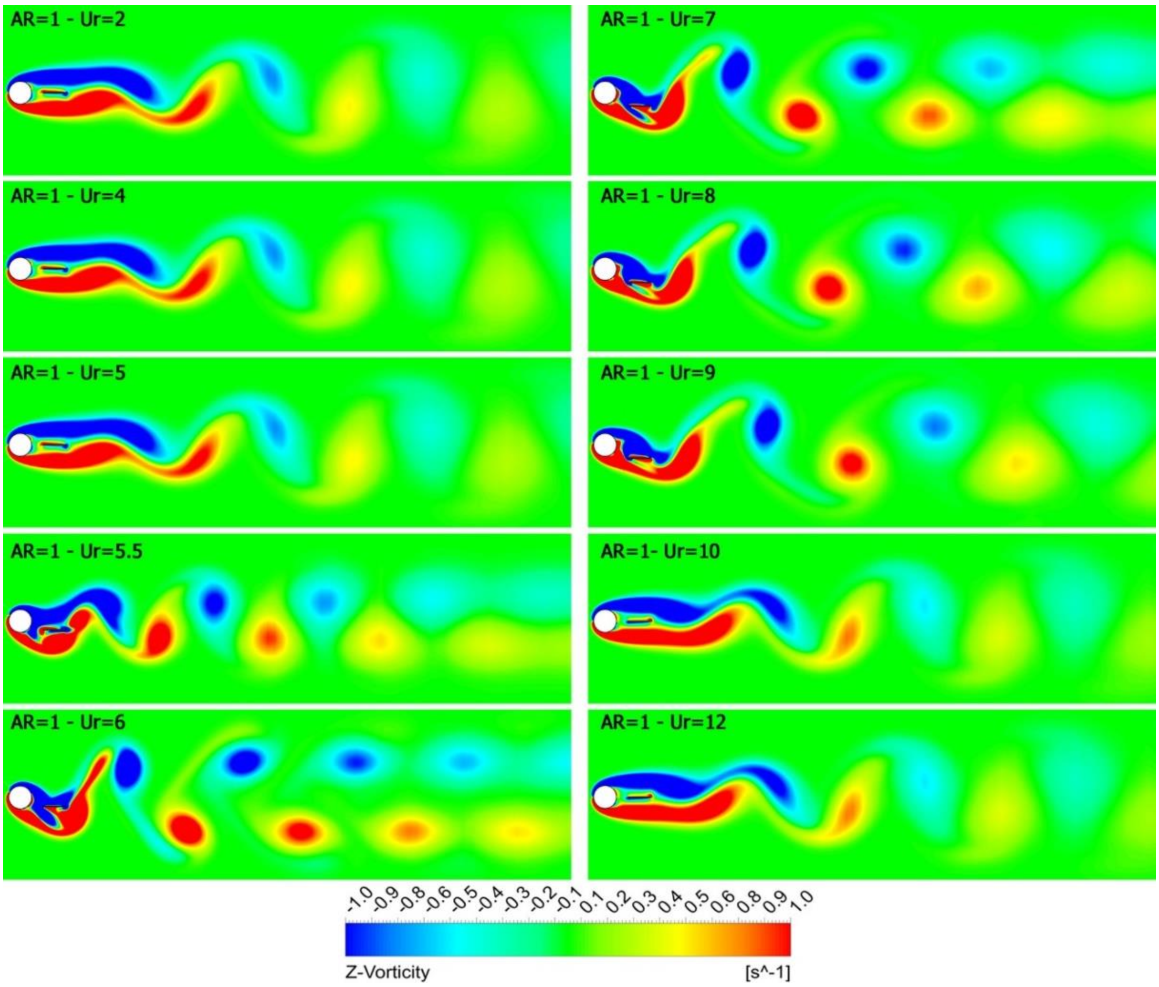

FIG. 16) Instantaneous non-dimensional vorticity contours in different reduced velocities for AR=1

By increasing the reduced velocity, an interaction between the shear layers and also the flat plate occurs, resulting in vortex shedding with a higher frequency and relatively near cores, each with a long arm stretched to the opposite side (U_r=5.5,6). Higher values of U_r diminish the interaction, and finally the vortex shedding is postponed again to the rear side of the plate, indicating the end of the synchronization regime and fall of vibration amplitude (U_r=10-12). When AR=0.75 (FIG. 17), the stretched shear layers' length is slightly shorter than those of AR=1 in small reduced velocities. Increasing the velocity initially results in forming the vortices around the plate and shedding two separated vortex streets with higher frequency (U_r=4.5). By U_r=5, shear layers will be confined between the objects, and vortices' stretched arms, although slightly weaker, appear from U_r=6. As the velocity increases (U_r=6-9), the interaction of shear layers weakens, and vortex formation gradually shifts to the upper and lower sides of the plate and finally moves further downstream (U_r=10-12).

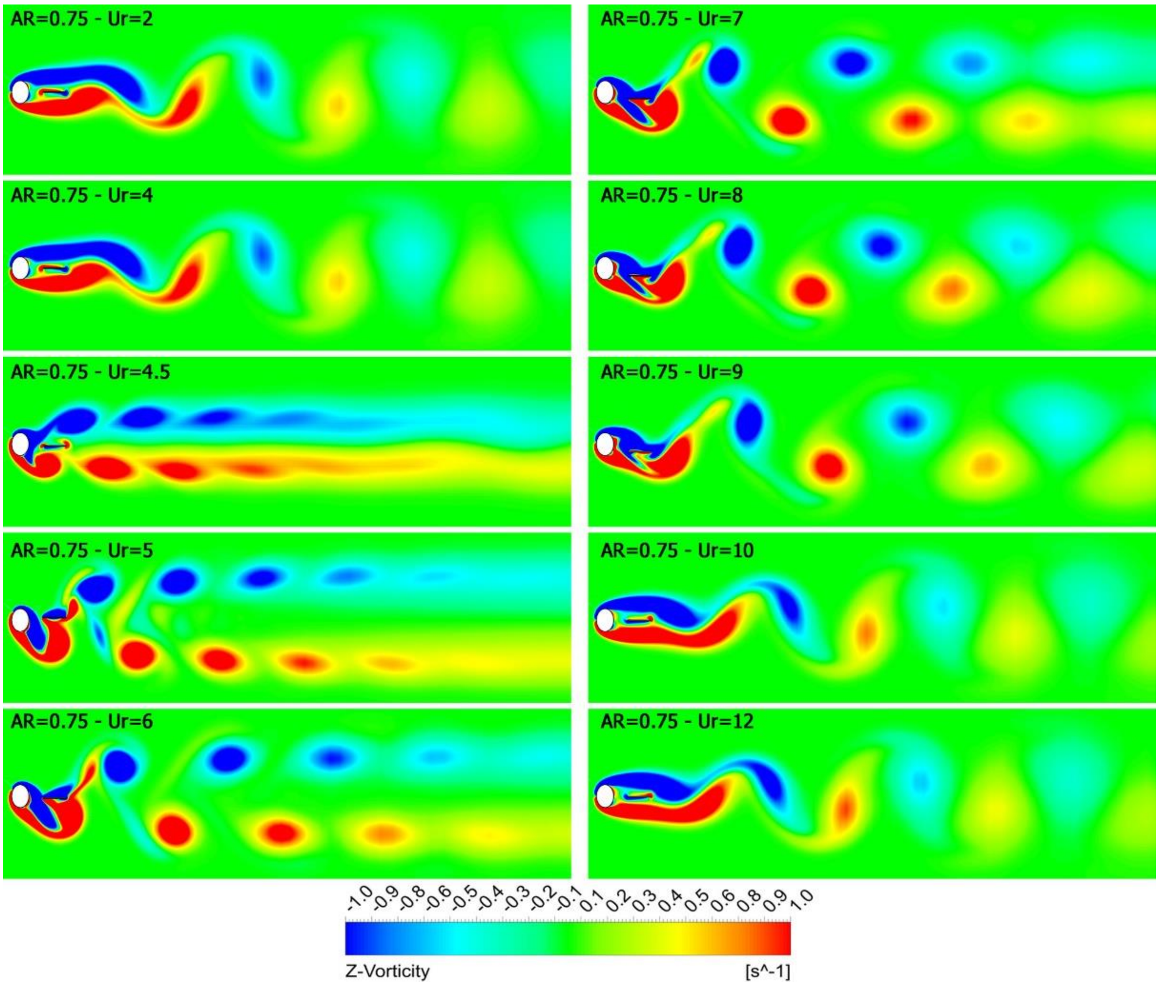

FIG. 17) Instantaneous non-dimensional vorticity contours in different reduced velocities for AR=0.75

Separated shear layers and postponed vortex shedding also appear in low reduced velocities for AR=0.5 (U_r=2) shown in FIG. 18. A periodic vortex shedding occurs on the plate's upper and lower sides, which merge downstream at U_r=3.5, 4. In higher velocities, as the vibration amplitude of the cylinder is considerably higher than the plate, the shear layers are vertically stretched, and the shedding process is found to be almost independent of the plate. Increasing the velocity from U_r=6 to 7, which includes a lower amplitude for the cylinder and a higher one for the plate, involves the flat plate in shedding process. This mechanism continues up to U_r=10, where the stretched shear layers appear again and shedding transfers completely to somewhere beyond the flat plate.

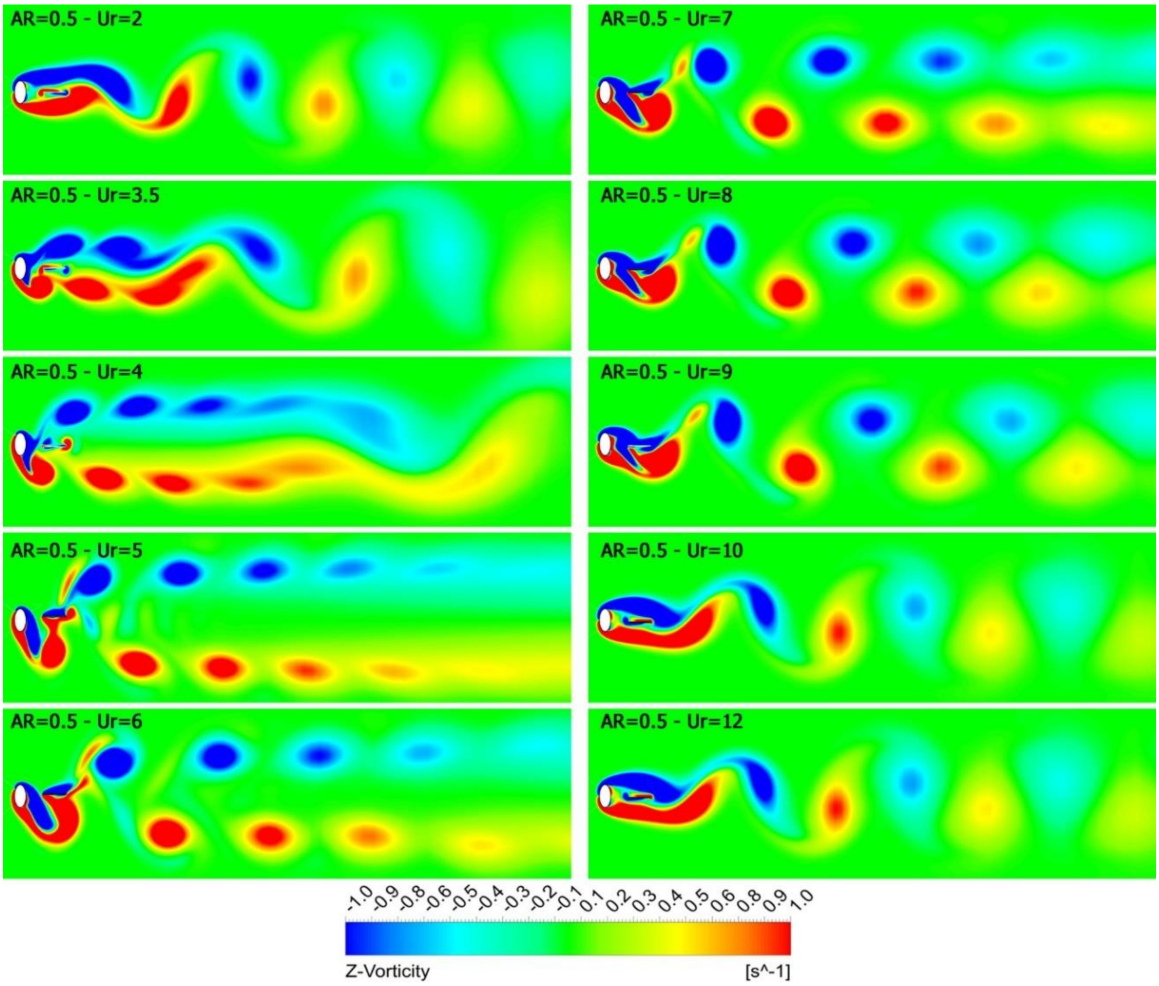

FIG. 18) Instantaneous non-dimensional vorticity contours in different reduced velocities for AR=0.5

The wake structure differs for the lowest AR (FIG. 19). The stretched shear layers and periodic vortices, which merge further downstream, also appear in this case (U_r=2,2.5 -3). The large vibration amplitude of the cylinder leads to extremely vertically stretched shear layers and little interaction with the flat plate (U_r=4-5-6). This flow structure results in two separated vortex streets with relatively far apart cores. Because of the wake instability, an interaction may occur between such vortex streets, which will finally be mixed and merged further downstream (U_r=4). This phenomenon was also reported by Vijay et al. for a bare elliptical cylinder (Vijay et al., 2020). As the presence of the flat plate has no considerable effect in these velocities, a similar vibration response is reasonable for the cylinder. The wake structure in higher reduced velocities is generally identical to those with high aspect ratios, and the vortex cores become closer to the wake centerline. Surprisingly, by increasing the velocity, the interaction of the shear layers and the flat plate continues, which conforms to the relatively high vibration amplitude of the objects.

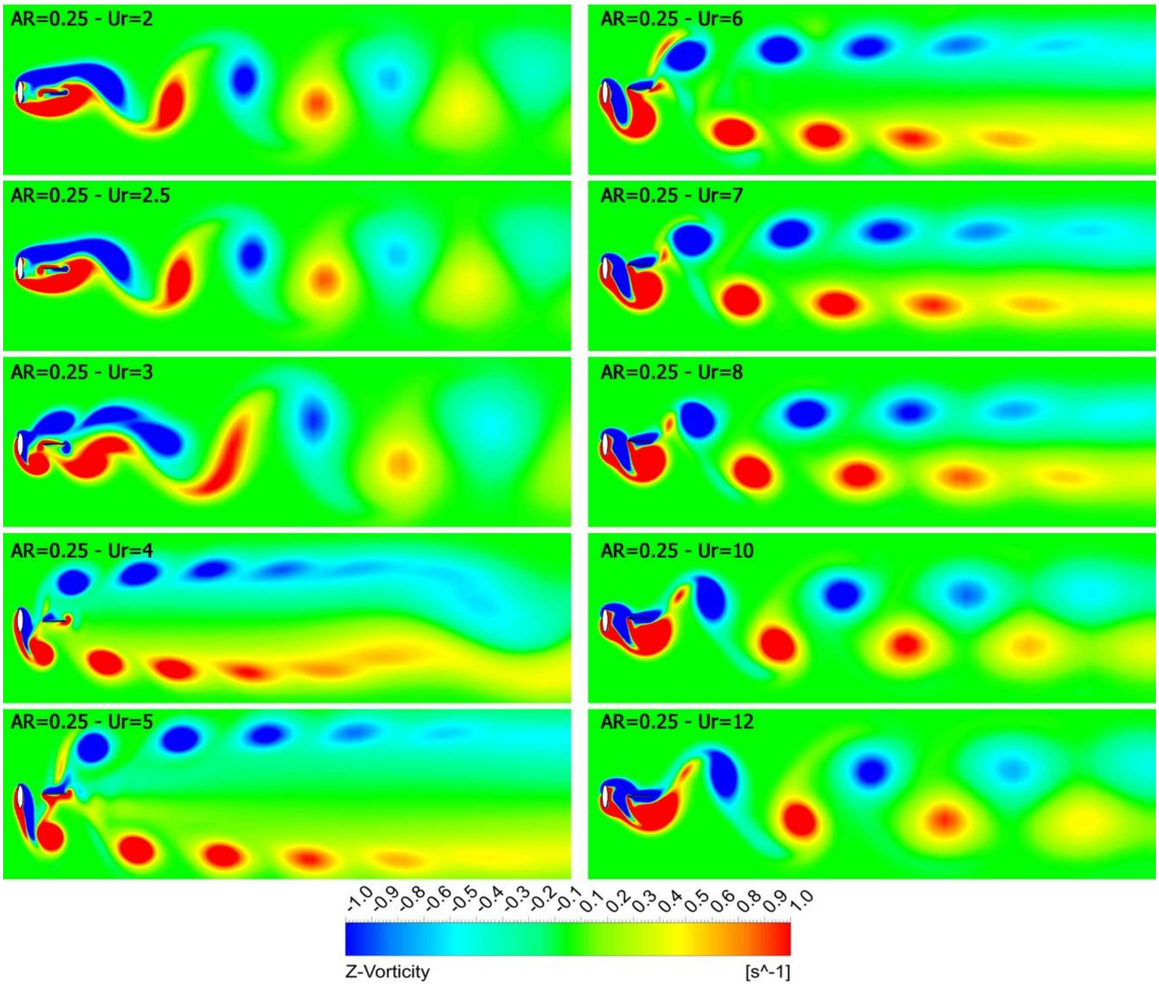

FIG. 19) Instantaneous non-dimensional vorticity contours in different reduced velocities for AR=0.25

As shown in FIG. 14, the presence of the flat plate reduces the lift of the upstream cylinder considerably in low reduced velocities and before the jump in vibration amplitude. FIG. 20 presents the variation of lift coefficient and pressure coefficient contours for different ARs in a low reduced velocity of U_r=2.

The presence of the flat plate that delays the vortex shedding by forming two stretched shear layers, shown in FIG. 16-FIG. 19, drastically reduces lift force variation during one cycle of vortex shedding for the cylinder. As shown in FIG. 20-a CL does not exceed 0.07 in any cases.

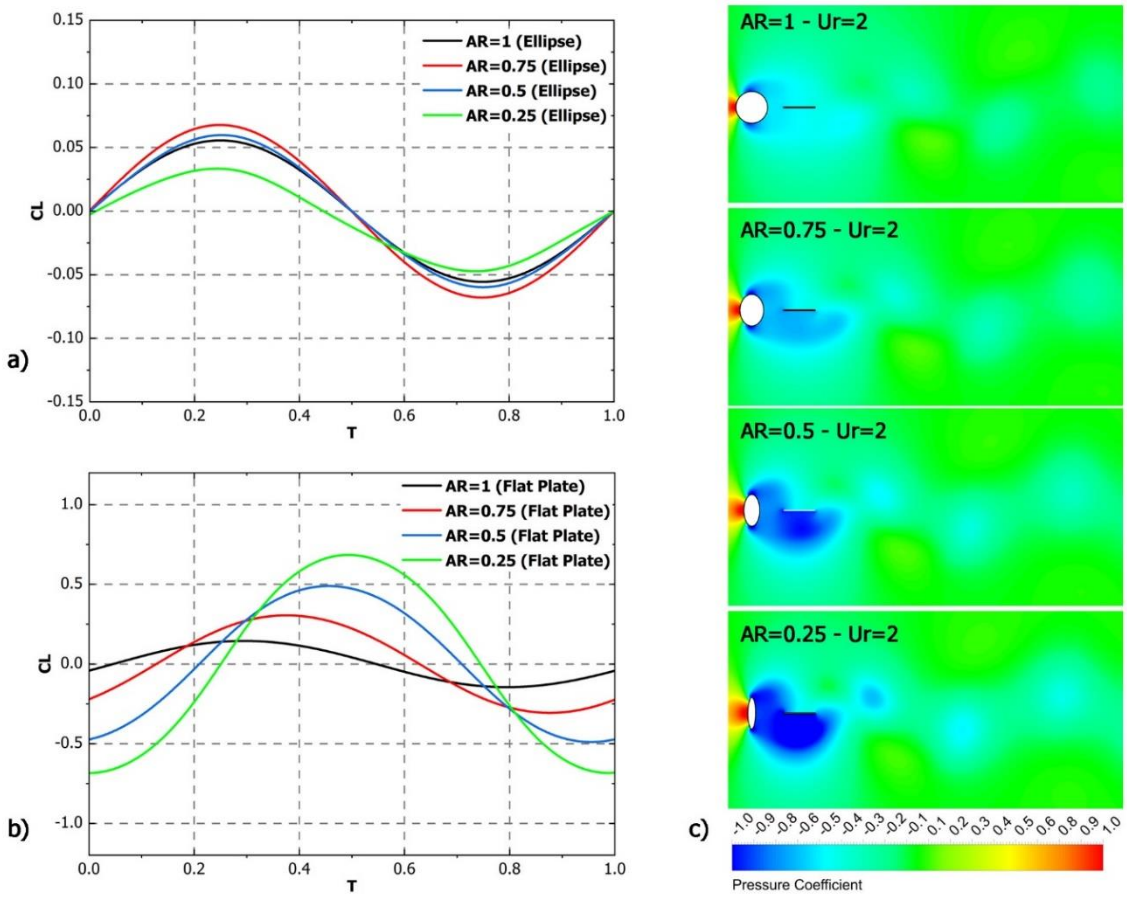

FIG. 20) Variation of lift coefficient for the Cylinder (a) and the flat plate (b) and pressure coefficient contours (c) at Ur=2

In a low aspect ratio, although the wake structure is generally similar with stretched and separated shear layers, it is a bit shorter, which leads to more interaction with the flat plate. As shown in FIG. 20-c, a periodic pressure variation appears around the plate; therefore, a higher lift coefficient is expected. The variation of CL around the plate (shown in FIG. 20-b) also confirms it. It is worth mentioning that as the vortex shedding frequency is far from the natural frequency, none of the objects vibrates at this reduced velocity.

The wake structure is also different for AR=0.25-Ur=12 (FIG. 19). In this case, the vortex shedding still occurs between the objects, resulting in a different wake, including periodic vortex shedding and local low-pressure zones around the objects (FIG. 21-c).

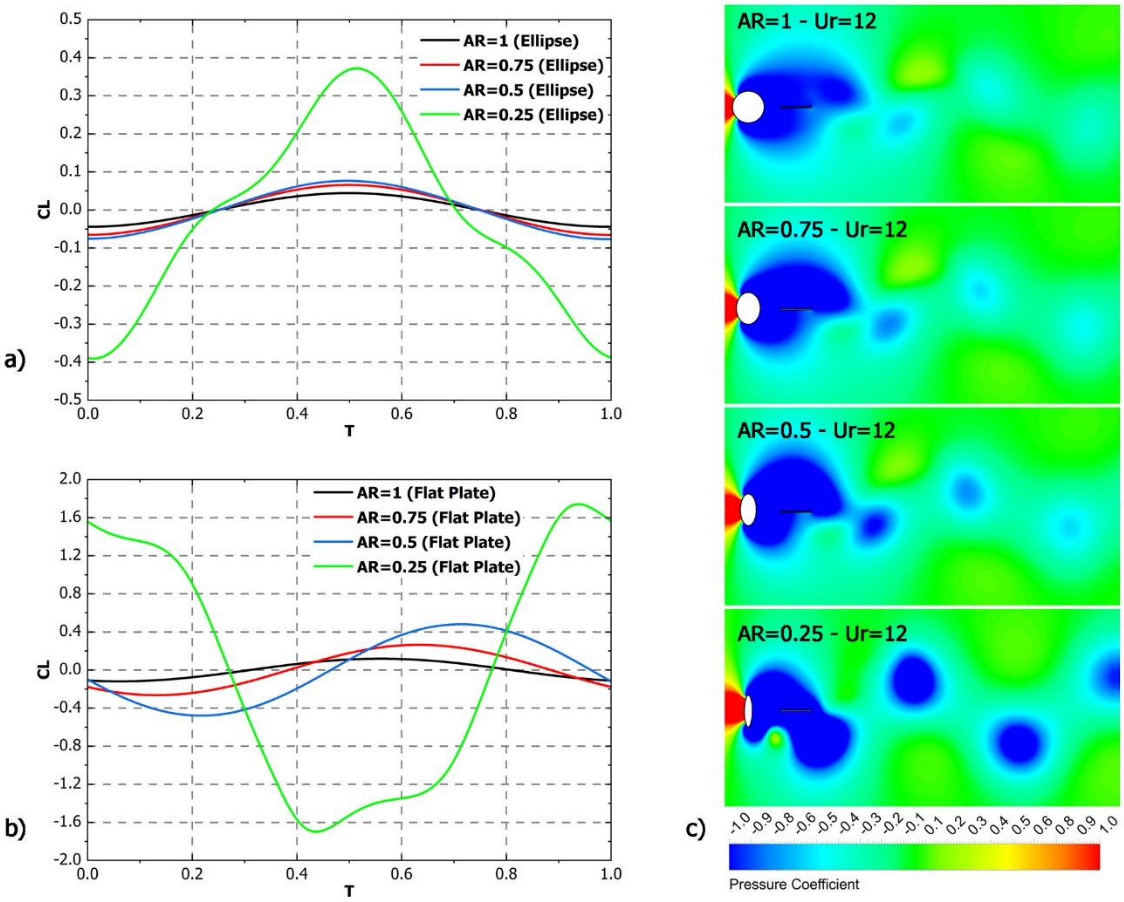

FIG. 21) Variation of lift coefficient for the Cylinder (a) and the flat plate (b) and pressure coefficient contours (c) at Ur=12

This structure exerts higher lift forces compared to the other cases. While the maximum lift coefficient for the upstream cylinder does not exceed CL=0.1 for AR=0.5-0.7-1 during one oscillation cycle, it reaches 0.4 for the lowest AR (FIG. 21-a). Similarly, for the flat plate, the variation of CL is found to be considerably higher in this case (FIG. 21-b).

5 Conclusion

Two dimensional numerical simulations were conducted in laminar flow to investigate the effect of a free-to-vibrate wake-mounted flat plate on the VIV of an upstream elliptical cylinder with a variable aspect ratio. The major/minor axis of the cylinder is defined perpendicular/aligned to the uniform flow and the plate's length is assumed to be equal to the major axis of the cylinder, which is constant in this study. The investigation includes six horizontal spacing values in the range of G=0.5-3 and four different aspect ratios (AR=0.25, 0.5, 0.75, 1), which are defined as the ratio of the minor axis over the major one. The Re number, based on the free stream velocity and major axis of the cylinder is set fixed at 100. A relatively low mass ratio of 10 is selected for the objects and the damping effect is assumed to be negligible ($\zeta = 0$). The following conclusions are drawn:

1. The presence of a flat plate can alter the wake structure behind an elliptical cylinder. Regardless of the cylinder's aspect ratio, reducing the horizontal gap between the cylinder and flat plate results in an amplification of vortex-induced vibration for the cylinder, particularly for small spacings. This amplification is due to changes in the shear layer structure caused by the flat plate, which leads to alterations in the pressure distribution around the cylinder. Additionally, it has been found that lower aspect ratios result in a higher amplification rate. Lowering the aspect ratio considerably reduces the maximum vibration for the flat plate, and the amplification of wake-induced vibration for the flat plate is limited to an aspect ratio of 0.25 and 1.

2. The phase difference of vibration between the objects is strongly correlated with the horizontal distance and the aspect ratio of the upstream cylinder. It varies linearly as the

horizontal distance changes, and reducing the AR moves the location of in-phase vibration towards the cylinder by shortening the vortex formation and shedding length.

3. A broader lock-in regime is observed for the cylinder in all aspect ratios when the flat plate is mounted at a short distance of G=0.5. Although the presence of the flat plate slightly delays the onset of the lock-in regime, the end of synchronization shifts to a higher reduced velocity. The flat plate follows the upstream cylinder at the beginning and end of the lock-in regime. While its amplitude remains relatively constant during synchronization, it drops considerably as the aspect ratio decreases.

4. The amplitude of the flat plate increases at reduced velocities associated with the initial response branch of the upstream cylinder. The lower vibration amplitude of the flat plate in lower aspect ratios is attributed to the different wake structures and reduced interaction between the shear layers and the flat plate.

The present study may be extended further to investigate the use of parallel flat plates in order to achieve higher vibration amplitudes for renewable energy applications. Future work could also consider the effects of mass ratio and Re number.

Declaration of competing interest

The authors declare that they have no known competing financial interests or personal relationships that could have appeared to influence the work reported in this paper.

Acknowledgment

"The authors acknowledge the use of the UCL Grace High Performance Computing Facility (Kathleen@UCL), and associated support services, in the completion of this work."

References

An, X., Song, B., Tian, W., Ma, C., 2018. Design and CFD simulations of a vortex-induced piezoelectric energy converter (VIPEC) for underwater environment. Energies 11, 330.

Apelt, C.J., West, G.S., Szewczyk, A.A., 1973. The effects of wake splitter plates on the flow past a circular cylinder in the range 104< R< 5× 104. J. Fluid Mech. 61, 187–198.

Armandei, M., Fernandes, A.C., 2016. Marine current energy extraction through buffeting. Int. J. Mar. Energy 14, 52–67.

Assi, G.R.S., Bearman, P.W., 2015. Transverse galloping of circular cylinders fitted with solid and slotted splitter plates. J. Fluids Struct. 54, 263–280.

Bearman, P.W., 1984. Vortex shedding from oscillating bluff bodies. Annu. Rev. Fluid Mech. 16, 195–222.

Bokaian, A., Geoola, F., 1984. Wake-induced galloping of two interfering circular cylinders. J. Fluid Mech. 146, 383–415.

Dehkordi, B.G., Jafari, H.H., 2010. On the suppression of vortex shedding from circular cylinders using detached short splitter-plates. J. Fluids Eng. 132.

Derakhshandeh, J.F., Alam, M.M., 2019. A review of bluff body wakes. Ocean Eng. 182, 475–488.

Faruquee, Z., Ting, D.S.K., Fartaj, A., Barron, R.M., Carriveau, R., 2007. The effects of axis ratio on laminar fluid flow around an elliptical cylinder. Int. J. Heat Fluid Flow 28, 1178–1189.

Gerrard, J.H., 1966. The mechanics of the formation region of vortices behind bluff bodies. J. Fluid Mech. 25, 401–413.

Hasheminejad, S.M., Jarrahi, M., 2015. Numerical simulation of two dimensional vortex-induced vibrations of an elliptic cylinder at low Reynolds numbers. Comput. Fluids 107, 25–42.

Henderson, R.D., 1997. Nonlinear dynamics and pattern formation in turbulent wake transition. J. Fluid Mech. 352, 65–112.

Hwang, J.-Y., Yang, K.-S., Sun, S.-H., 2003. Reduction of flow-induced forces on a circular cylinder using a detached splitter plate. Phys. Fluids 15, 2433–2436.

Jebelli, M., Masdari, M., 2022a. Interaction of free oscillating flat plate and VIV of a circular cylinder in laminar flow. J. Fluids Struct. 113, 103648. https://doi.org/https://doi.org/10.1016/j.jfluidstructs.2022.103648

Jebelli, M., Masdari, M., 2022b. Interaction of two parallel free oscillating flat plates and VIV of an upstream circular cylinder in laminar flow. Ocean Eng. 259, 111876.

Jiang, H., Cheng, L., Draper, S., An, H., Tong, F., 2016. Three-dimensional direct numerical simulation of wake transitions of a circular cylinder. J. Fluid Mech. 801, 353.

Johnson, S.A., Thompson, M.C., Hourigan, K., 2001. Flow past elliptical cylinders at low Reynolds numbers, in: 14th Australasian Fluid Mechanics Conference. Elsevier Adelaide, Australia, pp. 343–346.

Kawai, H., 1990. A discrete vortex analysis of flow around a vibrating cylinder with a splitter plate. J. Wind Eng. Ind. Aerodyn. 35, 259–273.

Kwon, K., Choi, H., 1996. Control of laminar vortex shedding behind a circular cylinder using splitter plates. Phys. Fluids 8, 479–486.

Nakamura, Y., Hirata, K., Kashima, K., 1994. Galloping of a circular cylinder in the presence of a splitter plate. J. Fluids Struct. 8, 355–365.

Ozkan, G.M., Firat, E., Akilli, H., 2017. Passive flow control in the near wake of a circular cylinder using attached permeable and inclined short plates. Ocean Eng. 134, 35–49. https://doi.org/https://doi.org/10.1016/j.oceaneng.2017.02.014

Ozono, S., 1999. Flow control of vortex shedding by a short splitter plate asymmetrically arranged downstream of a cylinder. Phys. Fluids 11, 2928–2934.

Paul, I., Prakash, K.A., Vengadesan, S., 2014. Numerical analysis of laminar fluid flow characteristics past an elliptic cylinder: A parametric study. Int. J. Numer. Methods Heat Fluid Flow.

Paul, I., Prakash, K.A., Vengadesan, S., Pulletikurthi, V., 2016. Analysis and characterisation of momentum and thermal wakes of elliptic cylinders. J. Fluid Mech. 807, 303–323.

Prasanth, T.K., Behara, S., Singh, S.P., Kumar, R., Mittal, S., 2006. Effect of blockage on vortex-induced vibrations at low Reynolds numbers. J. Fluids Struct. 22, 865–876.

Prasanth, T.K., Mittal, S., 2009. Vortex-induced vibration of two circular cylinders at low Reynolds number. J. Fluids Struct. 25, 731–741.

Prasanth, T.K., Mittal, S., 2008. Vortex-induced vibrations of a circular cylinder at low Reynolds numbers. J. Fluid Mech. 594, 463.

Radi, A., Thompson, M.C., Sheridan, J., Hourigan, K., 2013. From the circular cylinder to the flat plate wake: The variation of Strouhal number with Reynolds number for elliptical cylinders. Phys. Fluids 25, 101706. https://doi.org/10.1063/1.4827521

Roshko, A., 1955. On the wake and drag of bluff bodies. J. Aeronaut. Sci. 22, 124–132.

Sarpkaya, T., 2004. A critical review of the intrinsic nature of vortex-induced vibrations. J. Fluids Struct. 19, 389–447.

Stappenbelt, B., 2010. Splitter-plate wake stabilisation and low aspect ratio cylinder flow-induced vibration mitigation. Int. J. Offshore Polar Eng. 20.

Sun, X., Suh, C.S., Ye, Z.-H., Yu, B., 2020. Dynamics of a circular cylinder with an attached splitter plate in laminar flow: A transition from vortex-induced vibration to galloping. Phys. Fluids 32, 27104.

Vijay, K., Srinil, N., Zhu, H., Bao, Y., Zhou, D., Han, Z., 2020. Flow-induced transverse vibration of an elliptical cylinder with different aspect ratios. Ocean Eng. 214, 107831.

White, F.M., 1994. Fluid Mechanics, McGraw-Hill. New York.

Williamson, C.H.K., 1996. Three-dimensional wake transition, in: Advances in Turbulence VI. Springer, pp. 399–402.

Williamson, C.H.K., Govardhan, R., 2008. A brief review of recent results in vortex-induced vibrations. J. Wind Eng. Ind. Aerodyn. 96, 713–735.

Williamson, C.H.K., Govardhan, R., 2004. Vortex-induced vibrations. Annu. Rev. Fluid Mech. 36, 413–455.

Wu, J., Shu, C., Zhao, N., 2014. Numerical investigation of vortex-induced vibration of a circular cylinder with a hinged flat plate. Phys. Fluids 26, 63601.

Yogeswaran, V., Sen, S., Mittal, S., 2014. Free vibrations of an elliptic cylinder at low Reynolds numbers. J. Fluids Struct. 51, 55–67.

Zdravkovich, M.M., 1988. Review of interference-induced oscillations in flow past two parallel circular cylinders in various arrangements. J. Wind Eng. Ind. Aerodyn. 28, 183–199.

Zhang, M., Øiseth, O., Xu, F., 2021a. Laminar flow-induced vibration of a three-degree-of-freedom circular cylinder with an attached splitter plate. Phys. Fluids 33, 113605.

Zhang, M., Wang, X., Øiseth, O., 2021b. Torsional vibration of a circular cylinder with an attached splitter plate in laminar flow. Ocean Eng. 236, 109514.

Zhao, J., Hourigan, K., Thompson, M.C., 2019. Dynamic response of elliptical cylinders undergoing transverse flow-induced vibration. J. Fluids Struct. 89, 123–131.

Zhu, H., Liu, W., 2020. Flow control and vibration response of a circular cylinder attached with a wavy plate. Ocean Eng. 212, 107537. https://doi.org/https://doi.org/10.1016/j.oceaneng.2020.107537